Detailed isofield calorimetry of La(Fe,Si,Mn)H reveals distributed magnetocaloric phase transitions

Erbesdobler, Florian; Bahl, C. R. H.; Bjørk, Rasmus; Nielsen, Kaspar Kirstein

Published in:
Journal of Applied Physics

Link to article, DOI:
10.1063/1.5137790

Publication date:
2020

Document Version
Publisher's PDF, also known as Version of record

Journal of Applied Physics

Detailed isofield calorimetry of La(Fe,Si,Mn)H reveals distributed magnetocaloric phase transitions

Cite as: J. Appl. Phys. **127**, 095102 (2020); https://doi.org/10.1063/1.5137790
Submitted: 13 November 2019 . Accepted: 10 February 2020 . Published Online: 06 March 2020

F. Erbesdobler, C. R. H. Bahl, R. Bjørk, and K. K. Nielsen

Journal of Applied Physics ARTICLE scitation.org/journal/jap

Detailed isofield calorimetry of La(Fe,Si,Mn)H reveals distributed magnetocaloric phase transitions

Cite as: J. Appl. Phys. **127**, 095102 (2020); doi: 10.1063/1.5137790
Submitted: 13 November 2019 · Accepted: 10 February 2020 ·
Published Online: 6 March 2020

F. Erbesdobler,[a] C. R. H. Bahl, R. Bjørk, and K. K. Nielsen

AFFILIATIONS

DTU Energy Conversion and Storage, Technical University of Denmark, Frederiksborgvej 399, 4000 Roskilde, Denmark

Note: This paper is part of the Special Topic on Multicalorics.
[a]**Author to whom correspondence should be addressed:** floe@dtu.dk

ABSTRACT

We show that low ramp rate differential scanning calorimetry of the magnetocaloric material $La(Fe_{11.47}Si_{1.28}Mn_{0.25})H_{1.65}$ at different applied magnetic fields reveals the presence of distributed phase transitions. Experimentally, we find that with or without an applied magnetic field, samples show a distinct peak pattern in their heat capacity around the transition temperature ($T_t \approx 30\,^{\circ}C$), i.e., multiple heat capacity peaks occur as a function of sample temperature. Additionally, these reproducible patterns occur asymmetrically when heating and cooling. At finite applied fields higher than 0.15 T, we observe clearly distinguishable peaks of identical shape, albeit with different intensities. According to the latter, we re-identify the peaks under seven applied magnetic fields up to 1 T. We find that the peaks shift differently relative to each other as a function of field. In particular, for cooling experiments, the peak temperatures vary linearly in the field, although with different slopes. Through Bean–Rodbell (BR) modeling, we show that the experimentally observed behavior can be simulated by small decoupled variations in the BR parameters η and T_0, indicating a distributed composition of the magnetocaloric material.

I. INTRODUCTION

First-order phase transition (FOPT) magnetocaloric materials (MCMs) are interesting due to their giant magnetocaloric effect (MCE), which is observed as a temperature change with a change in the applied magnetic field.[1] Samples are magnetocalorically characterized by the isothermal entropy change, $\Delta s(H, T)$, and the adiabatic temperature change, $\Delta T_{ad}(H, T)$. These properties may be derived from isofield measurements of the specific heat capacity $c_{p,H}(T)$ as a function of sample temperature.[2]

An example of a FOPT is the isotropic volume change in La(Fe,Si) based alloys. The transition temperature (T_t) can be tuned by manganese doping[3] with full hydrogenation for crystal stability reasons.[4] Hence, La(Fe,Si,Mn)H compounds, specifically $La(Fe_{11.47}Si_{1.28}Mn_{0.25})H_{1.65}$ due to its T_t around room temperature, are interesting as a working material in magnetocaloric cooling devices due to their long term stability and composition of abundant and inexpensive elements.[5] The crystallographic modifications during the phase transition can introduce extra challenges concerning crystal purity, since stoichiometric impurities cause temperature gradients which, in first-order materials, result in stresses and, therefore, fatigue during long term operation.[6,7]

Modeling the influence of localized volumes slightly differing in stoichiometry within FOPT materials[8] may enable MCM producers to identify key parameters for their production technique, i.e., powder metallurgy,[4] which may lead to better MCMs. In the past few years, several groups have focused on accurate determination of the MCM's first-order character. The Bean–Rodbell (BR) model[9] offers a practical solution by assuming a linear dependence of the exchange coupling and the unit cell volume through the model parameter η,[10] known as the magneto-elastic coupling. For $\eta > 1$, the material exhibits a FOPT, and for $\eta \leq 1$, the phase transition is of second order. A way to determine the materials order experimentally is by considering the shape of their heat capacity peaks,[11] which occur during temperature ramping across the material's T_t in a differential scanning calorimeter (DSC). FOPT MCMs exhibit a latent heat peak, which is shifted toward higher temperatures with increasing applied field if their phase transition is between a ferromagnetic (FM) and a paramagnetic (PM) state.[2] Recent isofield DSC measurements of the above mentioned material as a function of temperature at low ramp rates (down to 0.06 K/min) revealed a detailed peak pattern of transition temperatures.[12] These peaks have been interpreted as independent motion events of the

phase boundary associated with the system's latent heat and were observed to be modulatable by applied magnetic fields.[13]

Here, by using low ramp rate calorimetry during continuous heating and cooling of a FOPT La(Fe,Si,Mn)H sample, we map out the phase change landscape when undergoing the FM to PM transition and vice versa. Calorimetry is performed as a function of an applied field, and the experimental results are compared with the BR model in order to identify the relevant BR parameters and their possible variations that may help interpret and explain the above mentioned peak pattern in theory.

II. EXPERIMENTAL

A. Setup and experiment

We use a custom DSC designed to impose a temperature profile on a sample in the milligram range. The details of the device can be found elsewhere.[14] Its two key features are the capability to do experiments at low temperature ramp rates down to ± 0.05 K/min and the option of varying the applied magnetic field via a concentric Halbach cylinder of permanent magnets.[15] A Pt100 sensor measures the temperature near the sample. In order to establish the sample temperature, we find the measured temperature where the DSC signal has the highest peak at two different ramp rates. Thereby, we are able to correct the ramp rate dependent temperature lag due to the finite heat transfer between the sample and the sensor. Two nominally identical Peltier elements measure the differential heat flux, which is the target quantity of DSC: one containing the sample and the other empty. In order to avoid heat losses due to convection, measurements are performed under high vacuum ($\sim 10^{-7}$ mbar). Two perpendicularly arranged hall probes (HHP-NU 1255 and 1774, Arepoc) measure the in-plane components of the applied magnetic field. The DSC temperature ramping starts at 298 K for all experiments and is set to maintain a rate of 0.05 K/min. The sample heats up to 316 K resulting in a paramagnetic reset of the material. Subsequently, the continuous cooling starts until the sample reaches 298 K again. Then, the magnetic field is increased before the next heating run. By recording the measured values every 2.5 s, we achieve a resolution of around 475 data points per kelvin. Figure 1 shows the heat capacity around the transition temperature while cooling as an example.

Mounting the magnet at its lowest field causes an applied magnetic field of about 0.02 T, which shifts the peak pattern slightly to higher temperatures while the number and intensity of the peaks remain. This effect is also seen in Ref. 12 in their study of isofield measurements during heating DSC runs. However, the cooling pattern shows that, even at this low field, not all peaks shift by the same amount (see arrow in Fig. 1 or supplementary material for dynamic view). The investigated applied magnetic fields, besides 0 and 0.02 T, were 0.16, 0.31, 0.45, 0.60, 0.73, 0.86, and 0.98 T. Due to the complex sample geometry, the internal demagnetization field of the sample cannot be determined and thus only the applied field is given in the following.

B. Materials

We investigated a flake-shaped $La(Fe_{11.47}Si_{1.28}Mn_{0.25})H_{1.65}$ sample, kindly supplied by Vacuumschmelze GmbH. The sample

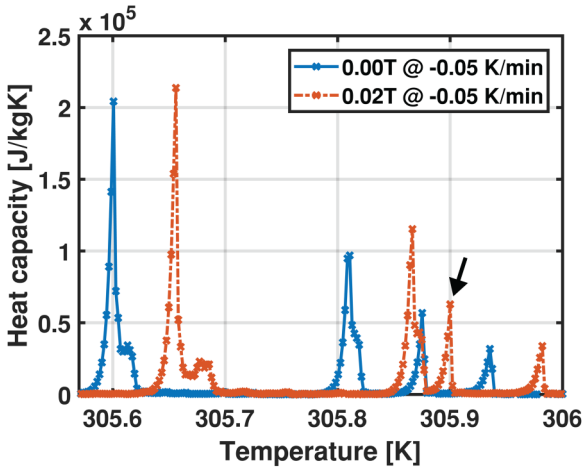

FIG. 1. Heat capacity peak pattern from a 2.64 mg of $La(Fe_{11.47}Si_{1.28}Mn_{0.25})H_{1.65}$ sample during a DSC experiment at -0.05 K/min ramp rate without applied field (blue) and a small magnetic field (red). The arrow denotes a peak that shifts less to the right than the rest.

weighs 2.64 mg and is shown in Fig. 2. The low mass ensures that the flake uniformly follows the device induced temperature ramp. The magnetic phase transition occurs nominally around 30 °C. Before and after the experiment the sample remained mechanically coherent, i.e., its shape and structural integrity were conserved throughout the experiment. We used thermal glue and vacuum

FIG. 2. Picture of $La(Fe_{11.47}Si_{1.28}Mn_{0.25})H_{1.65}$ flake (1×2.5 mm) glued to the measuring Peltier element of the DSC. The picture also shows the two perpendicular arranged Hall Probe sensors. The Pt100 sensor is glued in on the side with epoxy and thermal paste at the interface with the Cu-rod ensuring good thermal contact.

grease in order to gain sufficient thermal contact in the DSC and to prevent the sample from moving. The mass of the grease was determined by a subtractive method utilizing a standard lab scale. It turned out that grease alone is not sufficient to achieve sample immobilization due to the forces caused by frequent magnetic field variations. Hence, the estimated weight of the applied glue has been added to the grease mass, since their heat capacities are comparable. It amounts to maximal 10% of the joint masses of sample and grease. In order to calculate the sample's heat capacity, we measured the DSC signal of a 38.7 mg copper cube and took, respectively, the copper reference values according to Ref. 16. Above 300 K, we found the values by linear extrapolation.

C. Data analysis

The term "tracking" serves to describe the process of finding the same peak at different applied magnetic fields. Each respective peak pattern at a particular applied field denoted a "peak forest" in the following. The relative positions of the peak centers vary on the temperature axis as illustrated in Fig. 3 as a function of applied field.

In order to work out the relative variation for particular peaks, we additionally determine their temperature difference with respect to the most intense peak (Peak 0) at the respective applied field. In general, the intensity serves as the main criterion for re-identifying a specific peak at a different field. The selection of peaks is performed manually and their numbering (Peak 0 excluded) is only for labeling. In some cases, peaks overlap or have shoulders, which complicates the peak tracking. In these cases, which, in particular, occur during heating measurements, we do not identify the peaks. As an example, considering the right part of Fig. 3, it is clear that a fifth peak (Peak 4) is present at 0.98 T and additionally Peaks 1 and 3 have switched positions (see the supplementary material for a dynamic view).

In contrast, the multiple peak selection of Figs. 3 and 4 shows the tracking of only the most intense peak as a function of applied field. We obtain the depicted, corrected sample temperature by linearly extrapolating the peak temperatures, measured for ramp rates of ± 0.1 and ± 0.05 K/min, toward zero ramp rate. The extrapolated slopes are used to correct the peak forests, examined in the Results section (Fig. 5), for their thermal lag introduced by Pt100 to the sample distance. Moreover, the plot reveals the diminishing thermal hysteresis of our sample with respect to the magnetic field, as it is typical for first-order magnetocaloric materials.[3]

D. Modeling

We employ the well-known Bean–Rodbell (BR) model[9] in order to analyze the experimental results. The BR model is an extension of the Weiss mean field model[17] with the addition of assuming a linear coupling between the exchange constant and the volume change in the material. This coupling is often denoted by the magneto-elastic coupling and is assumed to be linear in the

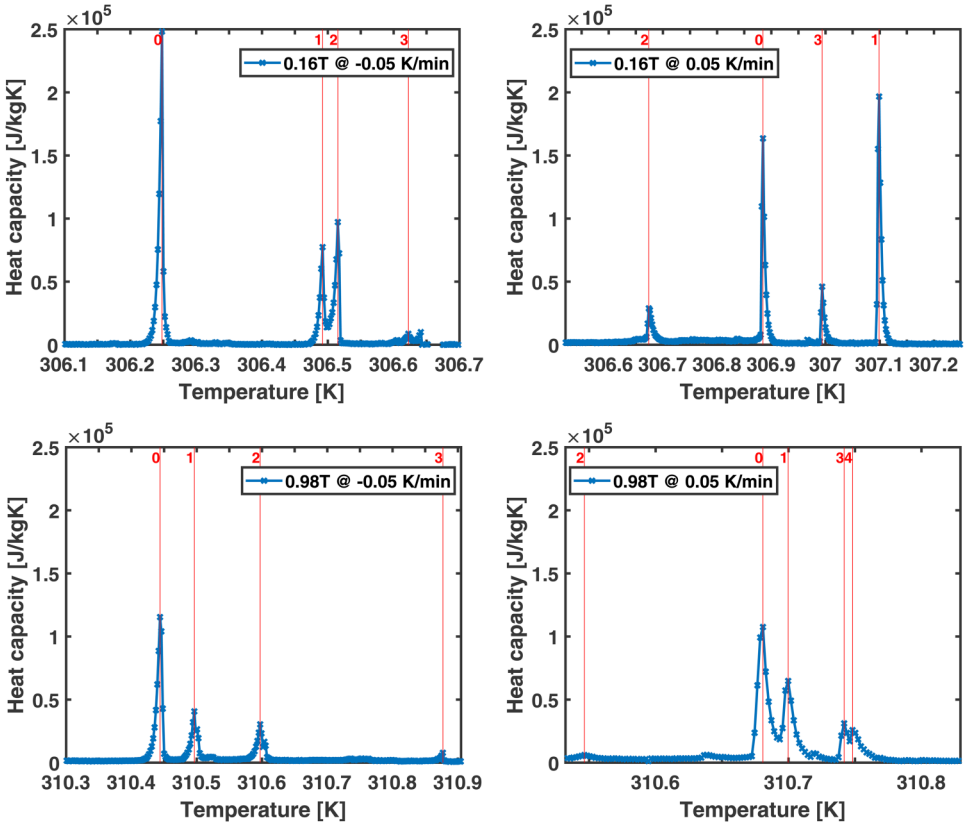

FIG. 3. Four peak forests with tracked peaks for heating at 0.16 T (right top), heating at 0.98 T (right bottom), cooling at 0.16 T (left top), and cooling at 0.98 T (left bottom).

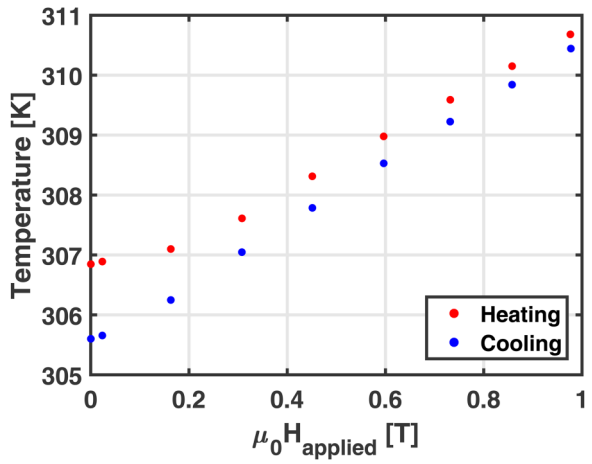

FIG. 4. The peak temperature of the most intensive peak as a function of the applied field.

volume change which in itself is assumed isotropic. The coupling is conventionally expressed through the parameter β,

$$T_t = T_0\left(1+\beta\frac{\Delta V}{V_0}\right), \tag{1}$$

with T_t denoting the transition temperature between ferromagnetic and paramagnetic phases. T_0 is the transition temperature the material would have in the absence of this coupling ($\beta = 0$). The volume in the absence of the magneto-elastic coupling is V_0 and $\Delta V = V - V_0$, with V denoting the actual volume of the sample. The sign of β is important if finite pressures are taken into account in the model. If the ambient pressure is assumed to be zero, then β only enters quadratically in the free energy,[18]

$$F = -k_B T\frac{N}{V_0}\ln\frac{\sinh\left(\frac{2J+1}{2J}\chi\right)}{\sinh\left(\frac{1}{2J}\chi\right)} + \frac{1}{2}\lambda_0\mu_0 M^2 + \frac{3}{8}\lambda_0^2\beta^2\kappa\mu_0^2 M^4, \tag{2}$$

with k_B denoting Boltzmann's constant; N, the number of spins; J, the spins' angular momentum; and $\chi = \frac{g\mu_B}{k_B T}J\left(H+\lambda_0(1+\frac{1}{2}\lambda_0\beta^2\kappa M^2)M\right)$, where g is the Landé factor, μ_B is the Bohr magneton, κ is the compressibility of the material, and $\lambda_0 = \frac{3T_0 k_B}{J(J+1)g^2\mu_B^2}\frac{V_0}{N}$. The equation above has been minimized with respect to volume analytically assuming zero pressure.[18] It also needs to be minimized with respect to magnetization, M, in order to yield the equilibrium solution(s). This is done numerically. When considering the BR model, it is often useful to define the parameter $\eta = \frac{40N}{V}\kappa k_B T\beta^2\frac{(J(J+1))^2}{(2J+1)^4-1}$. First, as β enters quadratically, its sign has no influence on η. Second, when $\eta > 1$, the transition is first order since there the magnetic entropy exhibits a finite jump, i.e., latent heat is present. When $\eta \leq 1$, the transition is second order. For $\eta > 1$, there may be two minima in the free energy as a function of magnetization. This is interpreted as hysteresis, i.e., the phase transition occurs at a higher temperature when going from a ferromagnetic state to a paramagnetic state (heating), while it occurs at a lower temperature when going from a paramagnetic to a ferromagnetic state (cooling).

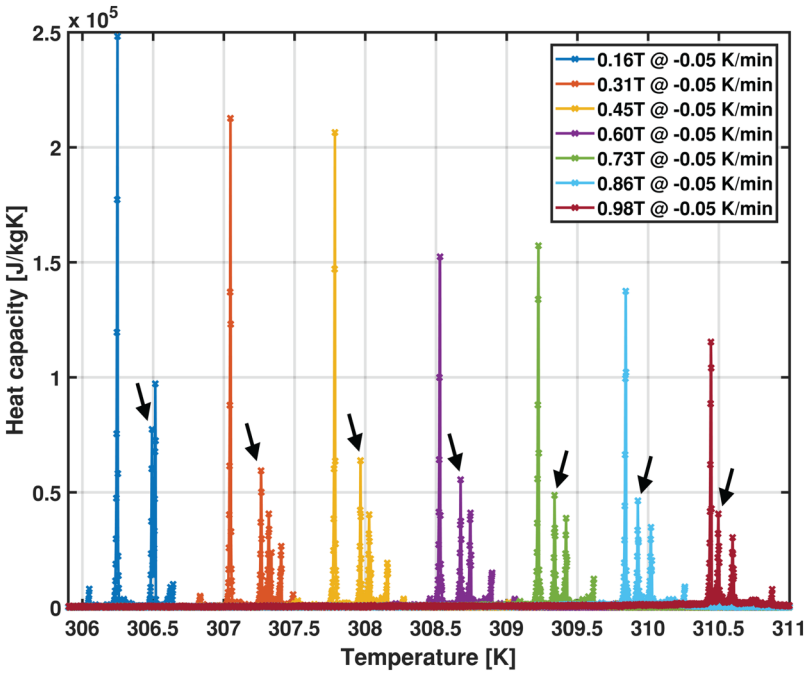

FIG. 5. Heat capacity peak patterns (seven peak forests) obtained during DSC cooling runs at −0.05 K/min ramp rate at different applied fields (shown in the legend). The black arrows point to a peak, which moves relative to its neighbors.

TABLE I. Summary of the parameters used in the BR model with their specific values assumed here. The values are selected to match those of La(Fe, Mn, Si)$_{13}$H type materials. The compressibility is taken from Ref. 19. It is noted that these values are similar to those used in Ref. 8.

Parameter name	Variable	Value
Magneto-elastic coupling	η_0	1.2
Total angular momentum	J	1
Curie temperature in the absence of magneto-volume coupling	$T_{t,0}$	306 K
Mass density	ρ	7200 kg/m^3
Number of magnetic ions per unit volume	N	6.04×10^{28} m^{-3}
Number of atoms per unit volume	N_{At}/V	7.39×10^{28} m^{-3}
Bulk compressibility	κ	7.3×10^{-12} Pa^{-1}
Debye temperature	T_D	350 K
Sommerfeld constant	γ_e	0.24 J/(kg K)^2
Pressure	p	0 Pa
Standard deviation of transition temperature	σ_{T_0}	0.05 K
Standard deviation of BR parameter	σ_η	0.05

The magnetic entropy is found through

$$S_{\mathrm{mag}} = \frac{k_B N}{V}\left(\ln\frac{\sinh\left(\frac{2J+1}{2J}\chi\right)}{\sinh\left(\frac{1}{2J}\chi\right)} - \chi B_J(\chi)\right), \tag{3}$$

with the Brillouin function

$$B_J(\chi) = \frac{2J+1}{2J}\coth\frac{2J+1}{2J}\chi - \frac{1}{2J}\coth\frac{1}{2J}\chi. \tag{4}$$

Finally, when considering the heat capacity of the system, the contributions from the lattice and the electrons also need to be included. We adopt the conventional Debye model for the lattice and the Sommerfeld model for the electronic contribution,

$$\begin{aligned} S_{\mathrm{lat}}(T) &= -\frac{3N_{At}}{V}k_B\left(\ln\left(1-e^{-\frac{T_D}{T}}\right) - 4D\left(\frac{T_D}{T}\right)\right), \\ D(\tau) &= \frac{1}{\tau^3}\int_0^\tau \frac{\chi^3}{e^\chi - 1}dx, \\ S_{\mathrm{ele}} &= \gamma_e T. \end{aligned} \tag{5}$$

The total entropy is then the superposition of the magnetic, lattice, and electronic entropies. The number of atoms per volume is $\frac{N_{At}}{V}$, the Debye temperature is T_D, and the Sommerfeld constant is γ_e.

The model parameters used are the unit cell volume in the absence of the magneto-elastic coupling, V_0, the corresponding transition temperature T_0, and η. These model parameters were chosen following Ref. 10, where the chemical inhomogeneity was modeled by varying T_0 through a Gaussian distribution with a standard deviation σ_{T_0}. Table I summarizes the model parameters and their values.

We model the sample as consisting of small non-interacting units of different size with slightly different properties expressed through variation in T_0 and η. These two variables are stochastically varied through a Gauss distribution with standard variations of $\sigma_{T_0} = 0.05$ K and $\sigma_\eta = 0.05$, respectively. The resulting heat capacity is assumed to obey the superposition principle expressed as a weighted sum of the individual units' heat capacities. In this way, we can mimic a sample with slightly varying properties.

III. RESULTS

A. Movement of peaks with field

As shown previously in Fig. 3, the peaks in heat capacity move with the applied field. In Fig. 5, we plot the cooling heat capacity as a function of sample temperature at several applied magnetic fields. This reveals that the peaks are moving relative to each other as a function of the applied field. The black arrow points to one of several peaks (denoted as "Peak 1" in the following) that can be consistently tracked for the different applied fields. Note that the peak moves relative to the surrounding peaks.

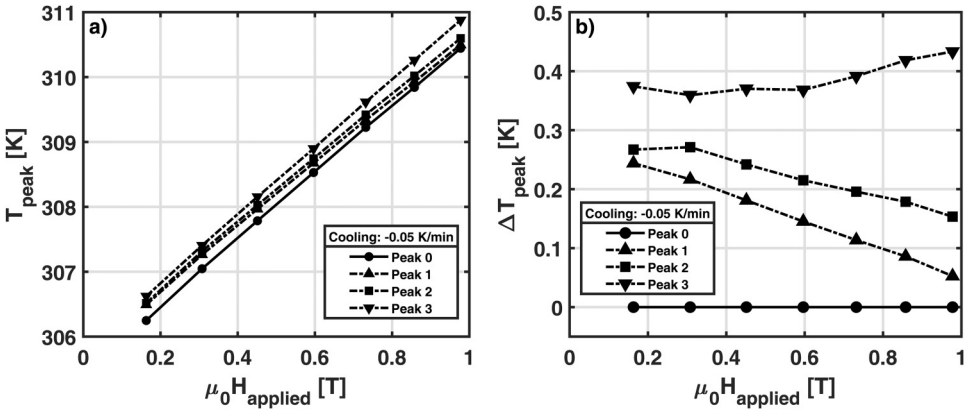

FIG. 6. Tracked temperatures for cooling peak patterns at −0.05 K/min for different applied magnetic fields. The peaks are subjectively numbered. (a) Absolute peak temperature. (b) Relative (to Peak 0) peak temperature.

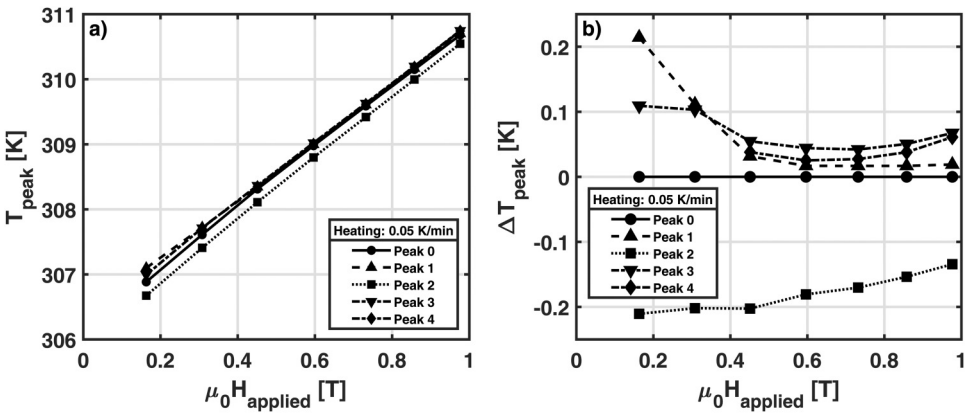

FIG. 7. Tracked temperatures for heating peak patterns at 0.05 K/min for different applied magnetic fields. The peaks are subjectively numbered. (a) Absolute peak temperature (b) Relative (to Peak 0) peak temperature.

As described above, the peaks in heat capacity are tracked as a function of temperature under different applied magnetic fields in the range from 0.16 to 0.98 T. At lower fields, here 0.00 T and 0.02 T, the peaks cannot be identified consistently with peaks at higher applied fields, and thus, these data are not shown in the following figures, but are included within the supplementary material. We assume lack of tracking to be caused by the presence of magnetic domains. As shown in Ref. 20, below a certain field, the presence of magnetic domains in low crystalline anisotropy samples makes the determination of the local field unreliable. For the investigated material, the reliability criterion reached above 0.15 T.[21]

Figure 6 shows the results of the systematic tracking process of all significant peaks in the absolute temperature scale (a) and relative to the intensive peak, Peak 0, (b) for cooling. By considering the peak propagation on the absolute temperature scale [Fig. 6(a)], we clearly observe the field-driven linear shift of all peak temperatures. Figure 6(b), however, shows that the peaks are moving relatively in opposite directions. Moreover, the absolute temperature does not entail a certain moving direction, i.e., peaks that occur in one peak forest at lower/higher absolute temperature do not respectively possess lower/higher slopes in the relative plot. Similar curves but for heating are shown in Fig. 7. The relative heating curves in Fig. 7(b) exhibit a linear trend most prominent for Peak 2, which is not close to the other peaks. For those peaks, the assumption of the linear trend seems to be only valid for fields lower than 0.45 T. Above 0.45 T, however, they start to diverge as was also observed by Basso *et al.*[3] Overall and in contrast to the cooling data, with increasing applied field, the peaks seem to condense to an absolute range of only 0.2 K from initially 0.42 K, which also makes the re-identification of the peaks more difficult.

Table II summarizes the linear shifts for different peaks on the absolute temperature scale [Figs. 6(a) and 7(a)]. Here, T_{init} accounts for the linearly extrapolated temperature at zero field for the respective, re-identified peak. From Table II, Figs. 6(a), and 7(a), the heating peak occurrences on the absolute temperature scale show similar linear trends as the cooling peaks with the difference of a slightly decreased slope. The hysteresis induced asymmetry of the *FMPM* phase transition explains this behavior, i.e., decreased latent heat induced peak shifts for the $FM \rightarrow PM$ compared to the $PM \rightarrow FM$ transition while exposed to an identical change in the applied field. The fact that for cooling higher T_{init} does not necessarily lead to higher slopes will be explained within the framework of the Bean–Rodbell model in Sec. III B.

Overall, we observe broad peak forests in heating and cooling, i.e., there are significant peaks that exist even farther away than 0.1 K from Peak 0 temperature. During heating, this situation seems to collapse at a magnetic field of 0.45 T, and thereafter, we find the largest peaks only very close to the most intense T_t peak (<0.1 K). During cooling, however, even at the highest applied field, i.e., 0.98 T, peaks still occur far from T_t (>0.1 K). Additionally, the shifts of the peaks behave linearly in the applied magnetic field but not identically. Every peak shifts through the field with its own slope or "speed," which seems to be also independent from the starting point at a low field in a way that peaks with ascending T_{init}s do not necessarily have ascending slopes.

TABLE II. Values of linear fit for tracked peaks on the absolute temperature scale. T_{init} denotes the y-intersection, and the 95% confidence intervals are given for T_{init} and the slopes of the linear fits for the cooling (c) and heating (h) peaks.

Peak No.	T_{init} (K)	Slope (K/T)	Peak No.	T_{init} (K)	Slope (K/T)
Peak 0c	305.45 ± 0.06	5.13 ± 0.09	Peak 0h	306.17 ± 0.08	4.65 ± 0.13
Peak 1c	305.74 ± 0.07	4.90 ± 0.10	Peak 1h	306.36 ± 0.03	4.44 ± 0.04
Peak 2c	305.75 ± 0.08	4.98 ± 0.12	Peak 2h	305.94 ± 0.07	4.74 ± 0.10
Peak 3c	305.79 ± 0.03	5.21 ± 0.05	Peak 3h	306.29 ± 0.05	4.58 ± 0.08
			Peak 4h	306.29 ± 0.04	4.55 ± 0.06

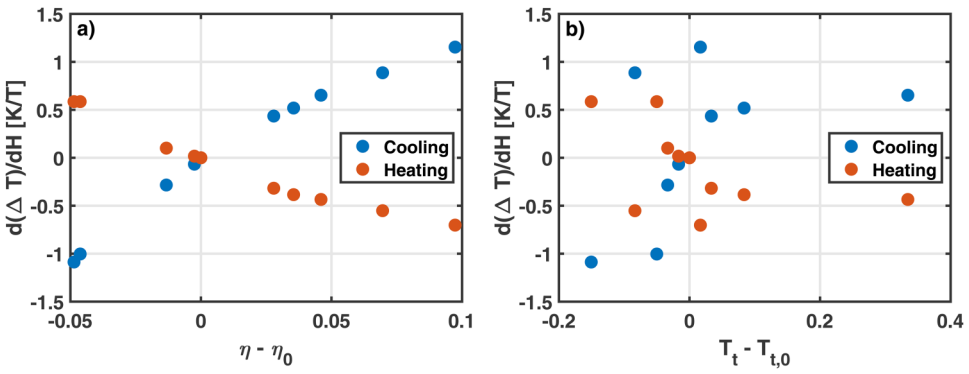

FIG. 8. Model results showing the difference in slope of the peak positions with respect to a peak arbitrarily chosen in the middle of the peak forest. (a) The slope difference as a function of difference in η and (b) the slope difference as a function of difference in T_t, both with respect to the selected peak reference.

To investigate if the relative movement of the peaks is a function of the ramp rate, we have also conducted measurements at a ramp rate of 0.1 K/min. The results here are consistent with those at 0.05 K/min and can be found in the supplementary material. The peaks show the same shape but lower overall intensities, whereas the intensity distribution is preserved. All corresponding peaks show the same kinetics, i.e., they rise and decay within the same times, independent of the maintained ramp rate. Thus, their first-order character shapes the heat capacity response and not instrumental features.

B. Modeling

With the model as described above and the associated parameters (Table I), the resulting slopes of peak forests consisting of 10 peaks were found through linear fits to the peak temperatures as a function of the applied field. One of the peaks was selected arbitrarily as a reference, and the change in slope with respect to the slope of this peak is given in Fig. 8, both as a function of the associated change in η [Fig. 8(a)] and the change in T_t [Fig. 8(b)].

Two points are immediately clear: first, the dependence of η is very pronounced and close to, but not exactly, linear. Second, the dependence of the change in slope with respect to the reference peak of the change in T_t is almost random. This indicates that both η and T_t may vary inside a sample over a narrow interval: the first parameter (η) in a very systematic way and the second (T_t) almost not systematically at all. This supports the experimental result given above (in particular, see Table II) that the degree of first orderness varies within a sample but does not follow the local peak temperatures (T_t).

Furthermore and in contrast to η, T_t does not exhibit distinctive symmetry with regard to heating and cooling. This is consistent with the experimental results.

IV. DISCUSSION

The results show that the phase transitions occur at different temperatures locally within the sample. This was already reported in Ref. 12. Upon heating, we qualitatively reproduce the experimental results as reported in Ref. 3. In contrast to the interpretation of Ref. 13, however, our combined modeling and experimental results indicate that "distributed phase transitions" perhaps do not originate from impurity induced variation but may be an effect of the sample composition, differences in shape, and composition of material grains, which may result in marginal stoichiometry variations throughout the sample. We have shown that the peak temperatures move at different speeds as a function of applied field upon cooling. This implies that not only does T_0 vary locally but so does η. This is supported by the BR model, where decoupled variation of T_0 and η showed exactly this. Our results have been controlled by investigating another sample from the same material batch, which showed qualitatively identical results.

It is of interest to consider to what degree T_0 and η, which in the experiment correspond to T_{init} and the peak temperature slope, are coupled. The answer is given in Table II, where the ascending T_{init} (T_0) values do not lead to ascending slope (η) values. Hence, the experiment reveals that η and T_0 are not strongly coupled for small variations.

V. CONCLUSION AND OUTLOOK

Through careful measurements of bulk $La(Fe_{11.47}Si_{1.28}Mn_{0.25})H_{1.65}$, we were able to consistently track heat capacity peaks at several different applied magnetic fields. As a function of field, we observed absolute and relative moving heat capacity peaks around the sample's transition temperature. In detail, we recorded and tracked the movement of four (five) peaks upon cooling (heating), respectively. At zero and low applied magnetic field, 0.02 T, the heat capacity peak pattern was domain dominated, which made consistent peak identification impossible.

We showed that BR modeling was capable of reproducing the relative peak moving behavior qualitatively and, to some degree, quantitatively. We conclude that a higher T_0 grain will, during an identical change of applied magnetic field, not necessarily result in faster moving peak temperatures compared to a lower T_0 grain. Indeed, both grains' peaks shift with field toward higher temperatures but do not show coupled relative movement. Hence, a grain can be modeled by an individual value of η, which accordingly was shown not to be a function of T_0 for local variations.

Since T_0 variation was already in the past associated with inhomogeneity, in particular, with regard to the Mn content, now the independent η variation requires physical interpretation. Spatially distributed grains, as they are inherent in polycrystalline samples, with different transition temperatures may be one possible explanation. Further effects could include internal stresses in the sample induced by varying properties, local field, and temperature.

SUPPLEMENTARY MATERIAL

See the supplementary material for the complete peak forests at different fields for heating and cooling at ± 0.1 and ± 0.05 K/min ramp rates.

ACKNOWLEDGMENTS

The authors wish to acknowledge the support of Alexander Barcza (Vacuumschmelze GmbH) and Jierong Liang (DTU Energy), respectively, for providing the sample and photos of the sample.

The authors also wish to acknowledge the financial support of the Independent Research Fund Denmark—Technologies and Productions Sciences (Project No. 7017-00034B).

DATA AVAILABILITY

The data that support the findings of this study are available within the article, its supplementary material (and additionally its supplementary material on dtu.data.dk).

REFERENCES

[1]F. Guillou, G. Porcari, H. Yibole, N. Van Dijk, and E. Brück, "Taming the first-order transition in giant magnetocaloric materials," Adv. Mater. **26**(17), 2671–2675 (2014).

[2]A. Smith, C. R. H. Bahl, R. Bjork, K. Engelbrecht, K. K. Nielsen, and N. Pryds, "Materials challenges for high performance magnetocaloric refrigeration devices," Adv. Energy Mater. **2**(11), 1288–1318 (2012).

[3]V. Basso, M. Piazzi, C. Bennati, and C. Curcio, "Hysteresis and phase transition kinetics in magnetocaloric materials," Phys. Status Solidi (B) Basic Res. **255**(2), 1700278 (2018).

[4]A. Barcza, M. Katter, V. Zellmann, S. Russek, S. Jacobs, and C. Zimm, "Stability and magnetocaloric properties of sintered $La(Fe,Mn,Si)_{13}H_z$ alloys," IEEE Trans. Magn. **47**(10), 3391–3394 (2011).

[5]V. Franco, J. S. Blázquez, B. Ingale, and A. Conde, "The magnetocaloric effect and magnetic refrigeration near room temperature: Materials and models," Annu. Rev. Mater. Res. **42**(1), 305–342 (2012).

[6]H. Neves Bez, K. K. Nielsen, A. Smith, P. Norby, K. Ståhl, and C. R. H. Bahl, "Strain development during the phase transition of $La(Fe,Mn,Si)_{13}H_z$," Appl. Phys. Lett. **109**(5), 051902 (2016).

[7]A. Gebert, M. Krautz, and A. Waske, "Exploring corrosion protection of La-Fe-Si magnetocaloric alloys by passivation," Intermetallics **75**, 88–95 (2016).

[8]K. K. Nielsen, C. R. H. Bahl, A. Smith, and R. Bjørk, "Spatially resolved modelling of inhomogeneous materials with a first order magnetic phase transition," J. Phys. D Appl. Phys. **50**(41), 414002 (2017).

[9]C. P. Bean and D. S. Rodbell, "Magnetic disorder as a first-order phase transformation," Phys. Rev. **126**(1), 104–115 (1962).

[10]H. N. Bez, K. K. Nielsen, P. Norby, A. Smith, and C. R. H. Bahl, "Magneto-elastic coupling in $La(Fe,Mn,Si)_{13}H_y$ within the Bean–Rodbell model," AIP Adv. **6**(5), 056217 (2016).

[11]J. Lyubina, "Magnetocaloric materials for energy efficient cooling," J. Phys. D Appl. Phys. **50**(5), 053002 (2017).

[12]C. Bennati, L. Gozzelino, E. S. Olivetti, and V. Basso, "Heterogeneous nucleation and heat flux avalanches in $La(Fe,Si)_{13}$ magnetocaloric compounds near the critical point," Appl. Phys. Lett. **109**(23), 231904 (2016).

[13]M. Piazzi, C. Bennati, and V. Basso, "Thermodynamics of the heat-flux avalanches at the first-order magnetic transition in magnetocaloric materials," Phys. Rev. Appl. **8**(4), 044023 (2017).

[14]K. K. Nielsen, H. N. Bez, L. Von Moos, R. Bjørk, D. Eriksen, and C. R. H. Bahl, "Direct measurements of the magnetic entropy change," Rev. Sci. Instrum. **86**(10), 103903 (2015).

[15]R. Bjørk, C. R. H. Bahl, A. Smith, D. V. Christensen, and N. Pryds, "An optimized magnet for magnetic refrigeration," J. Magn. Magn. Mater. **322**(21), 3324–3328 (2010).

[16]G. T. Furukawa, W. G. Saba, and M. L. Reilly, "Critical analysis of the heat-capacity data of the literature and evaluation of thermodynamic properties of copper, silver, and gold from 0 to 300 K," National Standard Reference Data Series—National Bureau of Standards 18, 1968.

[17]P. Weiss, "L'hypothèse du champ moléculaire et la propriété ferromagnétique," J. Phys. Théor. Appl. **6**(1), 661–690 (1907).

[18]A. Smith, K. K. Nielsen, and C. R. H. Bahl, "Scaling and universality in magnetocaloric materials," Phys. Rev. B **90**(10), 104422 (2014).

[19]K. Irisawa, A. Fujita, K. Fukamichi, M. Yamada, H. Mitamura, T. Goto, and K. Koyama, "Transition between antiferromagnetic and ferromagnetic states in itinerant-electron $La(Fe_xAl_{1-x})_{13}$ compounds," Phys. Rev. B **70**(21), 1–16 (2004).

[20]C. R. H. Bahl, A. Smith, and K. K. Nielsen, "The effect of magnetic domains on measurement of the magnetocaloric effect," in *Proceedings of the 6th IIF-IIR International Conference on Magnetic Refrigeration* (International Institute of Refrigeration, 2014), pp. 7–10.

[21]H. N. Bez, "Magnetocaloric materials and first order phase transitions," Ph.D. thesis (Department of Energy Conversion and Storage, Technical University of Denmark, 2016).